Journal of Sound and Vibration (1999) **227**(5), 935–948
Article No. jsvi.1998.2059, available online at http://www.idealibrary.com on IDEAL®

THE INFLUENCE OF RAILPAD STIFFNESS ON WHEELSET/TRACK INTERACTION AND CORRUGATION GROWTH

H. ILIAS
Institut für Luft- und Raumfahrt, *Technische Universität Berlin*, 10587 *Berlin*, *Germany*

(*Accepted* 22 *September* 1998)

The aim of the paper is to investigate the influence of the railpad stiffness on vehicle/track interaction and corrugation growth. For the structural dynamics of vehicle and track a time domain model is used which includes all relevant contact non-linearities. A simple wear model enables profile development calculations to be undertaken in the time domain by closing the feedback loop between a short-term dynamical process (structural dynamics) and a long-term damaging process (wear). The initial profile is taken from measurements of a ground rail. It is found that stiffer railpads lead to higher corrugation growth. The parametric excitation from passing sleepers is found to be important. For the chosen operational values this wavelength-fixing mechanism dominates the so-called final profiles of profile development calculations.

1. INTRODUCTION

When a train passes over a track having some kind of initial irregularity, varying contact forces are induced which cause irregularities at some wavelengths to grow, whereas others are unaffected or are suppressed. After several million wheelset passages, a more or less regular pattern called corrugation develops. This leads to increasing dynamic loads and therefore to increased maintenance. Since different types of corrugation have different explanations [1] this paper is restricted to short pitch corrugations due to high frequency, non-linear wheel/rail contact forces. Apart from the non-linear contact forces the longitudinal shift of contact point between wheel and rail is considered as a geometrical non-linearity.

Corrugation is considered to be a result of a wear feedback process coupling a short-term dynamical process of the structural dynamics with a long-term damage process (see Figure 1). By closing this feedback loop the profile development calculations are undertaken. The initial profile is taken from measurements of a ground rail. The main interest of this paper is in the influence of the railpad stiffness on contact forces and corrugation growth.

0022–460X/99/450935 + 14 $30.00/0

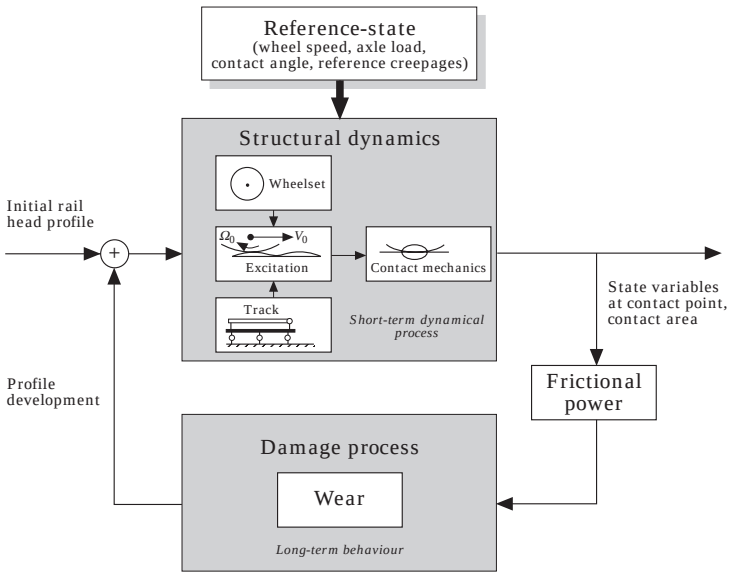

Figure 1. Model of feedback between structural dynamics and damage mechanism.

2. WHEELSET/TRACK INTERACTION MODEL

The vehicle is represented by a single wheelset, connected via primary springs and dampers to a rigid bogie, which is moving at constant speed over a short wavelength profile irregularity on the rail surface. For the vertical dynamics of the track a finite element model is used. The track model is effectively a closed ring (see Figure 2). The rail is modelled as a Timoshenko beam, which is discretely supported via viscoelastic railpads on rigid sleepers resting on a viscously damped elastic foundation. In order to simulate the effectively infinite

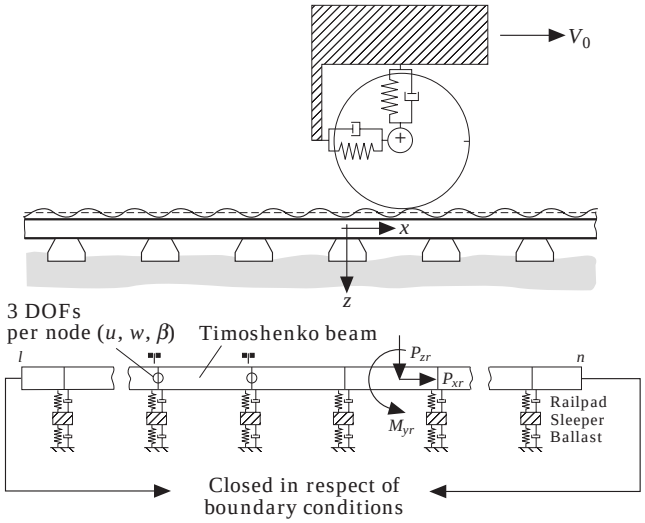

Figure 2. Wheelset/track model.

track the model contains a total of 30 sleepers. For the assumed track parameters this is sufficient for end effects to be negligible provided the pad damping is sufficiently high.

Lateral dynamics of the track are included simply by transforming receptances of the continuously supported rail into the time domain. All non-linearities are restricted to the modelling of the wheel/rail contact; the models of wheelset and track remain linear. The normal contact is represented by a non-linear Hertzian spring. For the non-linear but stationary tangential contact, the analytical, cubic approximation according to Shen *et al.* [2] is used. The irregular rail surface gives rise to a shift of the contact point relative to the point underneath the wheel centre at which the wheel would contact a smooth rail. This so-called geometrical shift of contact point is taken into account here and changes the profile irregularity which is actually noticed by the wheel. Another geometrical non-linearity is the contact patch filter, which reduces the influence of short wavelength profile irregularities and suppresses the influence of wavelengths smaller than the contact lengths in the rolling direction. The wheelset/track interaction model in detail can be found in reference [3].

2.1. INFLUENCE OF RAILPAD STIFFNESS ON THE VERTICAL RECEPTANCE OF THE TRACK

First of all, the influence of the pad stiffness on the vertical receptance of the track (with UIC60 rail and BW70 concrete sleeper) is investigated, since from this a better understanding of the dynamic behaviour of the linear track model can be gained. The pad stiffness is varied keeping the relaxation time (relation between stiffness and damping) constant. A soft pad then has less damping than a stiff pad. As well as the supposedly standard vertical pad stiffness of 280 MN/m a very stiff pad with a stiffness of 500 MN/m, a very soft pad with a stiffness of 60 MN/m and one with 180 MN/m is considered. The vertical receptance for the four different pad stiffnesses is calculated for a harmonically varying force which is fixed above the sleeper (see Figure 3 (left)) and at sleeper midspan (see Figure 3 (right)).

The frequency of the second resonance increases from about 250 Hz for the 60 MN/m pad to 600 Hz for the 500 MN/m pad. At this resonance the rail and sleepers oscillate almost in antiphase. The antiresonance between first and second resonances, at which the sleepers moving on the railpads act as a dynamic vibration absorber, gets more pronounced for increasing pad stiffness. This gives rise to a larger corrugation growth rate in the corresponding frequency range [4], since at antiresonances the system is dynamically stiff and therefore gives higher contact forces. The second quite shallow antiresonance at approximately 900 Hz appears for excitation above the sleeper. Here the rail vibrates with nodes almost at the sleepers. The second antiresonance becomes

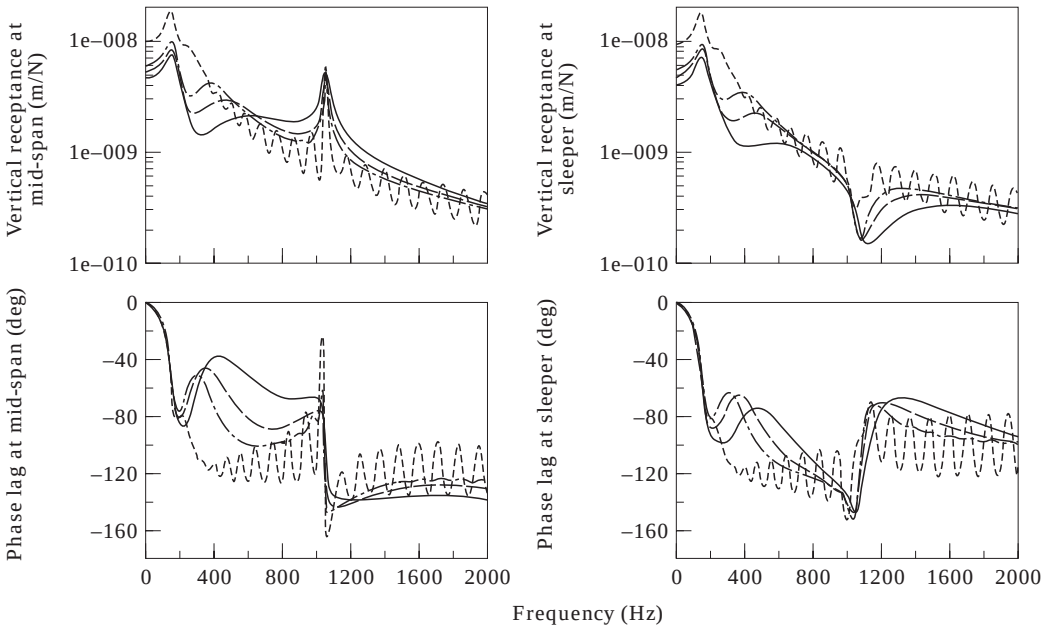

Figure 3 Vertical receptance for excitation above the sleeper (left) and at sleeper midspan (right) for four different pad stiffnesses (Mn/m): ——, 500; — —, 280; — - —, 180; – – –, 60.

more pronounced with decreasing pad stiffness because of the corresponding decrease in damping.

The changes at the pinned–pinned resonance frequency* for excitation at sleeper midspan are rather small. For excitation above the sleeper a third and most pronounced antiresonance occurs. With increasing pad stiffness the antiresonance shifts to higher frequencies and the related receptance decreases.

The oscillation in the receptances for the 60 MN/m pad is the effect of an inadequacy of the finite element (FE) model of the track, which is effectively a closed ring. The low damping of the 60 MN/m pad leads to circulating waves above 400 Hz. Clearly such waves would not exist in a real, essentially infinite, railway track. Even doubling the number of sleepers in the model is not enough to avoid these standing waves. Since the track's behaviour at the contact point is influenced by these standing waves, profile development calculations are unrealistic for the 60 MN/m pad. This illustrates why wheel/rail noise may be higher with more resilient pads: there is considerable transmission of waves along the rail and an increase in the effective radiating area of the rail. The lowest pad stiffness with sufficient pad damping for standing waves not to occur for the 30 sleeper model is 180 MN/m. Subsequent calculations with the 60 MN/m pad are believed to be reliable only up to about 400 Hz.

*At the so-called pinned–pinned frequency the rail oscillates sinusoidally with a wavelength of twice the sleeper pitch and nodes above the sleepers.

2.2. WHEEL/RAIL CONTACT FORCES AND FRICTIONAL POWER DENSITY

Next the influence of pad stiffness on the wheel/rail contact forces is investigated. The static wheel load is assumed to be 65·7 kN. A constant driving torque of 4600 Nm is applied to the wheelset which means for a wheel radius of 0·46 m and a coefficient of friction of 0·3 the tractive force is half the limiting traction μN_0. The inclination of the rail is chosen to be 1/40, so the lateral dynamics of the track are also excited.

As an initial profile a cosinusoidal profile irregularity with 5 μm amplitude and 30 mm wavelength is taken. The speed is varied between 4 m/s and 60 m/s in steps of 0.5 m/s: the excitation frequencies, f_{cp}, are thus in the range 133–2000 Hz. The sleeper passing frequency, f_{sp}, is in the range 6·7–100 Hz.

In Figure 4 the variation of maximum, minimum and mean values of the normal contact force with speed are shown. These values are taken from the time history of the normal contact force for a quasi-steady state solution. There are no very pronounced maxima for the higher pad stiffnesses. The normal contact force for the 60 MN/m pad has a quite distinct peak at the pinned–pinned resonance. Results for the 60 MN/m pad are believed to be reliable only up to about 400 Hz (12 m/s; see Figure 3). The very prominent peak in the contact force at the pinned–pinned resonance (or more correctly at the corresponding antiresonance) arises because of the exceptionally low damping in this mode of the ring model of the track.

The normal force increases with increasing frequency. The force is greatest at about 38–43 m/s: i.e., 1267–1433 Hz (the precise frequency depends on the pad's

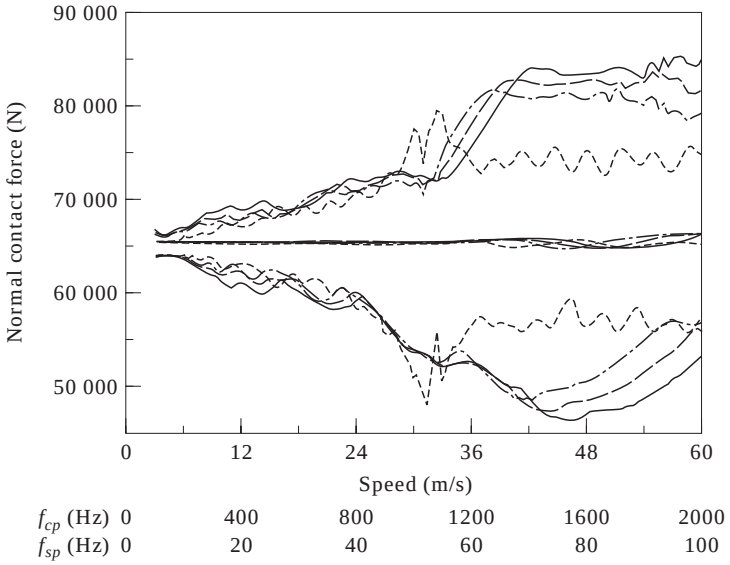

Figure 4 Maximum, miniumum and mean values of the normal contact force for four different pad stiffnesses (MN/m): ——, 500, — —, 280; — - —, 180, – – –, 60. Cosinusoidal initial profile with $\lambda = 30$ mm, $\Delta z = \pm 5$ μm.

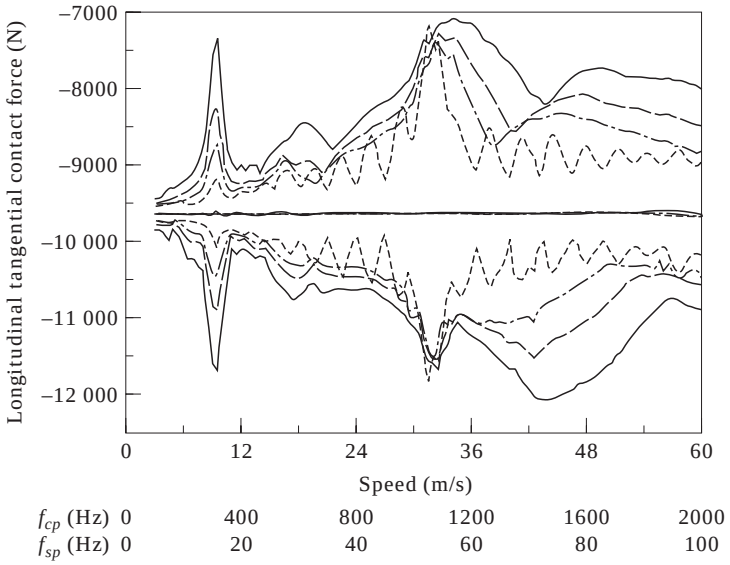

Figure 5. Maximum, minimum and mean values of the longitudinal tangential contact force for four different pad stiffnesses (MN/m): key as Figure 4. Cosinusoidal initial profile with $\lambda = 30$ mm, $\Delta z = \pm 5$ μm.

stiffness). In this speed range, there is a strong modulation of the contact force because the fundamental system resonance (at 68 Hz for the 280 M/m pad) is excited by passing sleepers. It is perhaps surprising that the highest amplitudes of contact force are not associated with the pinned–pinned resonance (and its associated antiresonance). Up to 1000 Hz and for frequencies above 1500 Hz the normal contact force is bigger for stiffer pads. Around the pinned–pinned frequency the soft pads cause higher normal contact forces because of the low damping, since the pinned–pinned mode itself is very lightly damped.

The longitudinal tangential contact force in dependency of speed for the 280 MN/m pad (see Figure 5) has maxima at approximately 300 Hz (the second rotational system antiresonance of bending), 600 Hz (two times the second rotational system antiresonance of bending, non-linear effect), and 1070 Hz (the pinned–pinned resonance).

Resonances and antiresonances of vertical and rotational receptances due to bending generally coincide. The first vertical resonance of track for the 280 MN/m pad is at 145 Hz, the second at 456 Hz and the first antiresonance at approximately 300 Hz (see Figure 3). Due to the higher effective mass the system resonances and antiresonances for a track with wheelset or vehicle is shifted to lower frequencies. So the first vertical system resonance is at 68 Hz and the first vertical system antiresonance is shifted to 240 Hz [5]. The rotational system resonances of bending are located at higher frequencies than the vertical system resonances because of the lower effective wheel mass in respect of rotation [6].

No variation with speed of either the lateral tangential contact force or the spin moment is shown. These are similar to the normal contact force.

Fluctuations of the lateral tangential contact force are one magnitude of order lower than those of the longitudinal tangential contact force.

The global or mean frictional power density, $p_R(t)$, is a measure of the energy loss in the wheel/rail contact. For a quasi-steady state solution it is defined as the product of creep forces and related relative velocities in the contact point, divided by the contact area, πab:

$$p_R(t) = -(v_m/\pi a(t)b(t))(T_x(t)\nu_x(t) + T_y(t)\nu_y(t) + M_z\phi_z(t)). \tag{1}$$

Clearly the mean frictional power density is proportional to the speed of the wheel. For the assumed parameters the factor of proportionality is $k = 6{\cdot}845 \times 10^{-8}$ Ws/m^3; the mean value for 60 m/s therefore is 4·107 W/mm^2. The mean value of the frictional power density is independent of pad stiffness.

In Figure 6 is shown the maximum frictional power density when the mean value, which increases linearly with speed, is substracted. Over almost the entire frequency range the stiffer pads lead to higher frictional power densities. This influence is quite strong in the frequency range up to about 900 Hz, quite small around the pinned–pinned frequency and very strong for frequencies above about 1500 Hz. Relative maxima for the supposedly standard pad of 280 MN/m are at approximately 300 Hz (twice the rotational system antiresonance of bending), 600 Hz (two times the second rotational system antiresonance of bending, non-linear effect), 680 Hz (10 times 68 Hz (first vertical system resonance), non-linear effect), 1070 Hz (pinned–pinned resonance), 1200 Hz (five times 240 Hz (first vertical system antiresonance), non-linear effect), and 1700 Hz (approximately 7×240 Hz, 25×68 Hz).

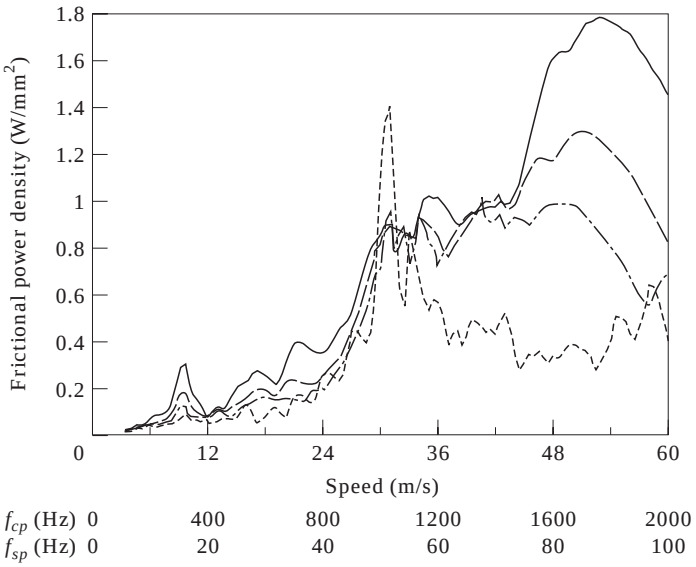

Figure 6. Maximum of the frictional power density for four different pad stiffnesses (MN/m): key as Figure 4. Cosinusoidal initial profile with $\lambda = 30$ mm, $\Delta z = \pm 5$ μm

Due to the geometrical contact non-linearities, integer multiples of the sleeper and corrugation passing frequencies are also excited. A variation of wavelengths of a cosinusoidal profile irregularity with constant wheel speed and a variation of wheel speed with a cosinusoidal irregularity of constant wavelength lead to different behaviour [3]. Clearly, for constant speed the sleeper passing frequency is constant, whereas for the variation of vehicle speed the sleeper passing frequency also varies and gives a second excitation frequency. If the sleeper passing frequency coincides with a system resonance, there may be a relatively high response. This behaviour is not represented in Hempelmanns linear corrugation model [4], which accordingly gives different results at those frequencies and speeds where this behaviour is significant [7].

3. WEAR CALCULATIONS

For profile development calculations in the time domain, simple wear models are required to reduce computation time. According to the *frictional power hypothesis*, the wear between wheel and rail is proportional to the product of creep forces transmitted between both bodies and the related relative velocities in contact point. For the sake of simplicity the material removal is associated here with a single point towards the rear of the contact patch, since the frictional power is only effective in the sliding area [3]. The point with which the wear is associated is assumed to be

$$e_R = \int_{-a_g}^{a_g} s(x_g)q(x_g)x_g \, dx_g \Big/ \int_{-a_g}^{a_g} s(x_g)q(x_g) \, dx_g, \tag{2}$$

where e_R is shown in Figure 7. The distribution of shear stress, $q(x_g)$, and the microslip, $s(x_g)$, are according to Carter's theory [8]. The point the wear is associated with is at the trailing edge ($e_R = -a$) for complete stick and $e_R = -a/4$ shifted backwards from the centre of the contact patch for complete slip (see Figure 7). This simplified wear calculation gives reasonable results providing the contact patches are approximately elliptical. This was shown in references [3, 7, 9] where comparisons with results obtained by Kalker's computer program CONTACT [10] are carried out.

Quasi-steady state time histories of the frictional power density are used to calculate the wear distribution in the longitudinal direction. A kind of contact

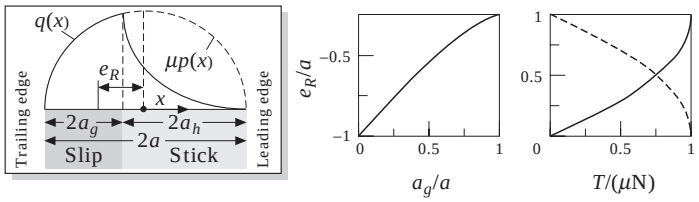

Figure 7. Left: notation within contact area. Centre: wear associated point in dependence of the microslip area. Right: microslip and stick area in dependence of creep force. ——, a_g/a; – – –, a_h/a.

filter is used in order to suppress the development of irregularities smaller than the contact length in the rolling direction.

4. PROFILE DEVELOPMENT/CORRUGATION GROWTH

The process of corrugation formation involves the closure of the feedback loop shown in Figure 1. The initial railhead profile is taken from measurements of a newly ground rail (see Figure 8). It is assumed that this profile is repeated for each sleeper bay. This initial profile excites the structural dynamics of the wheelset/track system. The wear in one sleeper bay is calculated by using contact forces and creepages or the frictional power density, respectively, of a quasi-steady state solution. The number of wheelset passages, N_k, required in order to give a 5% change of height of the profile at the location of maximum wear is calculated. The new profile of the rail head, η_{k+1} is then determined by linear extrapolation:

$$\eta_{k+1}(x) = \eta_k(x) - N_k \Delta z(x). \tag{3}$$

The changed rail head profile gives a new input for the structural dynamics in the next feedback loop of the calculation procedure. This feedback procedure is stopped when the normal contact force due to excitation with the worn profiles becomes so large that the wheel loses contact. This profile is regarded as the "final profile".

The profile development calculations are performed for a driven wheelset (constant driving torque of 4600 Nm) with a radius of 0·46 m. The speed of the wheelset is 32 m/s. The corresponding sleeper passing frequency (53 Hz) is quite close to the first system resonance for which wheelset, rail and sleepers oscillate approximately in phase.

First the profile development for a 280 MN/m pad is performed by using the initial profile from Figure 8 (see Figure 9, left). Each curve shows the resulting

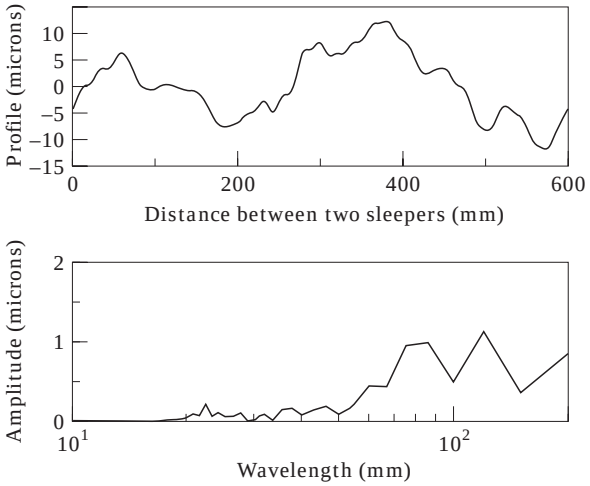

Figure 8. Initial profile.

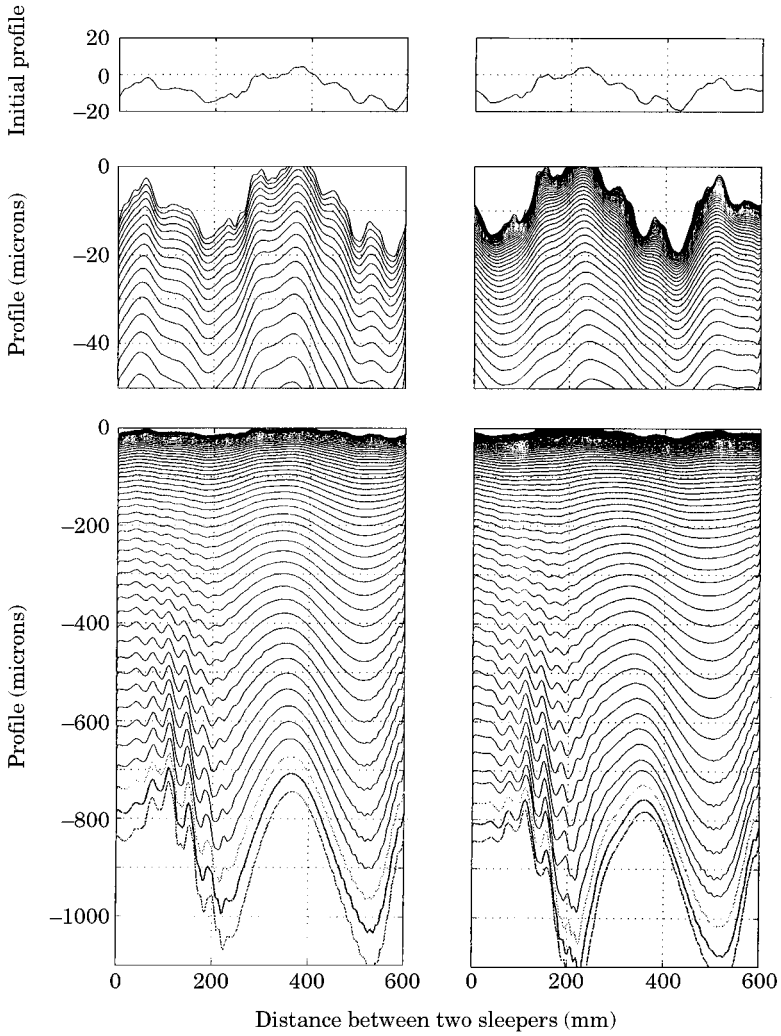

Figure 9. Profile development calculations for a pad stiffness of 280 MN/m. The speed is 32 m/s. Left: initial profile from Figure 8. Right: initial profile 180° phase shifted.

profile of one feedback loop. Starting from the initial profile the long wavelength corrugation of half the sleeper pitch (300 mm) grows. Simultaneously the rail wears constantly downwards and the short wavelength corrugation of the initial profile is worn away. Then shorter wavelength corrugations develop starting from the sleepers and shift slowly into the sleeper bay. The wear pattern of the final profile is fairly regular. Wear maxima are at about 250 mm and 550 mm.

The corrugation of 300 mm wavelength is related to the rotation of the smooth rail due to bending, which gives a relative velocity in the "nominal contact point"* [3] in the longitudinal direction of

$$\nu_x(t)v_m = z_s\dot{\beta}(t), \tag{4}$$

*The nominal contact point is the point where the wheel contacts the smooth rail.

where $\nu_x(t)$ is the elastic creepage in longitudinal direction, v_m is the mean speed of the wheelset, z_s is the distance between the centroid of the rail and the centre of the crown of the rail and $\dot{\beta}(t)$ is the time derivative of rotation of the rail at the nominal contact point. This dominant 300 mm wavelength was already included in the initial profile but develops also when it is not included in the initial profile to start with [9]. This is therefore a mechanism giving a corrugation of fixed wavelength (half the sleeper spacing) which is not dependent on vehicle speed. Whether such corrugations exist in practice could be ascertained from profile measurements on track with different sleeper spacings.

It is extremely interesting to examine the change in rail profile when the rail is moved so that the initial profile is 180° out of phase with that examined previously (see Figure 9, right). The maxima of the initial profile are now located at the minima of the frictional power density and *vice versa*. It now takes much longer for the corrugation to develop. The reason for this is that the system must first shift the maxima of the long wavelength corrugation to the position determined by the structural dynamics. When this is done, corrugations start to develop at shorter wavelengths. Thereafter, the profiles on the left and right sides in Figure 9 are very similar.

The final profiles for three different vertical railpad stiffnesses (180 MN/m, 280 MN/m, 500 MN/m) together with the corresponding amplitude spectra are shown in Figure 10. These final profiles have been obtained after subtracting the mean value of the wear z_0. This is equivalent to a constant material removal and is taken as negative downwards. Also given in Figure 10 is the required total number of wheelset passages N to get to these final profiles. The ratio between amplitudes of certain wavelengths of the final profile, $a(\lambda)$, and the total number

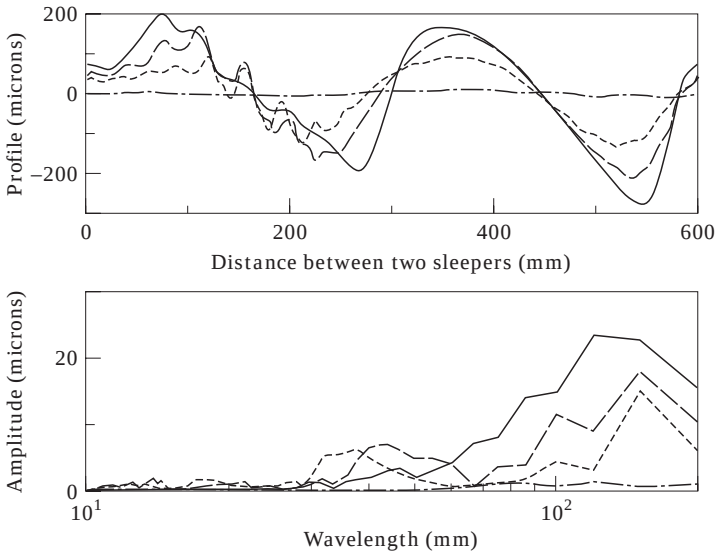

Figure 10. Final profiles for three different railpad stiffnesses; initial profile from Figure 8. — · —, Initial profile; – – –, c_z = 180 MN/m, Z_0 = −849 μm, N = 9·83 mio; — —, c_z = 280 MN/m, Z_0 = −841 μm, N = 9·66 mio; ——, c_Z = 500 MN/m, Z_0 = −686 μm, N = 7·64 mio.

TABLE 1
Amplitudes and wear rates for different wavelengths of the final profile

	$\delta = a(\lambda)/N$					
	c_z = 180 MN/m N = 9·83 mio		c_z = 280 MN/m N = 9·66 mio		c_z = 500 MN/m N = 7·64 mio	
λ (mm)	δ (μm/10^6)	$a(\lambda)$ (μm)	δ (μm/10^6)	$a(\lambda)$ (μm)	δ (μm/10^6)	$a(\lambda)$ (μm)
$\lambda \to \infty$	86·37	849	87·06	841	89·79	686
30–50	0·16	6	0·72	7	0·52	4
100	0·41	4	1·14	11	1·96	15
150	1·53	15	1·86	18	3·01	23
300	6·41	63	10·87	105	16·36	125

of wheelset passages, N,

$$\delta = (a(\lambda)/N) \quad [\mu m/\text{million wheelset passages}],$$

is a kind of wear rate.

Wear rates for different wavelengths and the three different railpad stiffnesses, taken from the results of Figure 10, are shown in Table 1. The constant wear rate $\delta(\lambda = \infty) = z_0/N$ changes very little for the three different pad stiffnesses since it is mainly dependant on the reference creepage and the vehicle speed. The biggest differences in the wear rates are obtained for the wavelengths of 100 mm and 300 mm. Compared with the supposedly standard pad of 280 MN/m, the wear rate for 100 mm wavelength increases by 72% for the 500 MN/m pad and decreases by 64% for the 180 MN/m pad. For 300 mm wavelength the wear rate compared with the 280 MN/m pad increases by 51% for the 500 MN/m pad and decreases by 41% for the 180 MN/m pad. In the short wavelength range (30 mm–50 mm) the wear rate for the 500 MN/m pad is lowest and for the 280 MN/m highest: 28% higher than for the 500 MN/m pad. However, the content of short wavelengths corrugation is very small, mainly because the amplitudes of short wavelength irregularities in the initial profile are very small. There is almost no 30 mm corrugation included in the initial profile (see Figure 8) which would excite the pinned–pinned resonance at the chosen speed of 32 m/s.

The parametric excitation from passing sleepers is important, particularly when this excites a system resonance [9]. In all final profiles shown in Figure 10 corrugations with a wavelength of half the sleeper spacing (i.e., 300 mm) dominate. Due to the non-linearities in the system, integer multiples of the sleeper passing frequency (53 Hz) are excited and lead to periodic wear at wavelength, of about 150 mm and 100 mm. The 100 mm corrugations are also related to the second rotational system antiresonance of bending, which gives a relative maximum in the frictional power density (see also Figure 6).

5. CONCLUSIONS

A quite sophisticated structural model for vehicle and track together with a quite simple wear model enables profile development calculations to be undertaken in the time domain. The influence of railpad stiffness on vehicle/track interaction and corrugation growth is investigated. The influence of pad stiffness on the vertical receptance of track is greatest up to about 600 Hz.

The frictional power density increases with increasing pad stiffness. This influence is quite large for frequencies up to 900 Hz, very small around the pinned–pinned frequency and biggest for frequencies above 1500 Hz. However, short wavelength corrugations corresponding to the highest frequencies are suppressed by the contact filter used for the wear calculation.

It appears that stiffer pads lead to higher differential wear rates and therefore to faster corrugation growth. For the chosen parameters and the initial profile, which has very small amplitudes of short wavelength irregularities, this influence is bigger for wavelengths of half the sleeper pitch or fractions of half the sleeper pitch, respectively. Parametric excitation from the discrete support is therefore important and dominates the final profiles. Due to the contact non-linearities, the 300 mm corrugation of half the sleeper pitch is overlaid with irregularities of 150 mm and 100 mm wavelength. Therefore it is clear that a non-linear corrugation model, especially in combination with the consideration of the excitation through passing sleepers, can lead to different final profiles from those which would be found using a linear corrugation model.

The corrugation growth rate depends on the phase of the initial profile related to the sleepers. If the phase lag of initial irregularity does not fit to the structural dynamics, the irregularity first moves to the "correct" position in the sleeper bay. This process greatly extends the time required for corrugation development. This possibility offers an extremely original, albeit perhaps impractical, means of delaying corrugation development.

It would be desirable to examine measurements of longitudinal rail profiles for different sleeper spacings to determine the extent to which corrugation does indeed develop with a wavelength of half the sleeper pitch.

ACKNOWLEDGMENTS

The author would like to thank Loram Rail Ltd. for providing the railhead profile measurements used in the paper as initial profile and Dr. Stuart L. Grassie for valuable comments and discussions.

REFERENCES

1. S. L. Grassie and J. Kalousek 1993 *Proceedings of the Institute of Mechanical Engineers, Journal of Rail and Rapid Transit* **207**, 57–68. Rail corrugation: characteristics, causes and treatments.
2. Z. Y Shen, J. K. Hedrick and J. A. Elkins 1983 *Proceedings of the 8th IAVSD Symposium, Cambridge, MA*, 591–605. A comparison of alternative creep force models for rail vehicle dynamic analysis.

3. H. ILIAS 1996 *VDI Fortschritt-Berichte, Reihe 12, Nr. 297. Düsseldorf: VDI-Verlag*. Nichtlineare Wechselwirkungen von Radsatz und Gleis beim Überrollen von Profilstörungen.
4. K. HEMPELMANN 1994 *Short pitch corrugation on railway rails—a linear model for prediction*. VDI Fortschritt-Berichte, Reihe 12, Nr. 231. Düsseldorf: VDI-Verlag.
5. B. RIPKE 1995 *Hochfrequente Gleismodellierung und Simulation der Fahrzeug-Gleis-Dynamik unter Verwendung einer nichtlinearen Kontaktmechanik*. VDI Fortschritt-Berichte, Reihe 12, Nr. 249. Düsseldorf: VDI-Verlag.
6. S. L. GRASSIE, R. W. GREGORY and K. L. JOHNSON 1982 *Proceedings of the Institute of Mechanical Engineers* **24**, 97–102. The dynamic response of railway track to high frequency longitudinal excitation.
7. A. IGELAND and H. Ilias 1996 in *Proceedings of the 2nd Mini Conference on Contact Mechanics and Wear of Rail/Wheel Systems, Budapest* (editor I. Zobory). Railhead wear calculations based on high frequency wheelset/track interaction—a comparison between different models.
8. F. W. CARTER 1926 On the action of a locomotive driving wheel. *Proceedings of the Royal Society of London* **A112**, 151–157.
9. A. IGELAND and H. ILIAS 1997 *Wear* **213**, 90–97. Rail head corrugation growth predictions based on non-linear, high frequency vehicle/track interaction.
10. J. J. KALKER 1986 *User's Manual of the* FORTRAN IV *Program* CONTACT. Delft University of Technology, Department of Mathematics and Computer Science.